Electronic Supplementary Material (ESI) for Physical Chemistry Chemical Physics.

Supplementary Information

Tunnel junction sensing of TATP explosive at the single-molecule level

Aleksandar Ž. Tomović,[a] Helena Miljkovic, [a,b] Miloš S. Dražić, [a] Vladimir P. Jovanović [a] and Radomir Zikic [a,*]

[a] University of Belgrade, Institute for Multidisciplinary Research, Kneza Višeslava 1, 11030 Belgrade, Serbia

[b] Present address: Laboratory of Nanoscale Biology, Institute of Bioengineering, Ecole Polytechnique Federale de Lausanne (EPFL), Lausanne, 1015, Switzerland

* Radomir Zikic. E-mail: radomir.zikic@sanu.ac.rs

1. Binding energies of different TATP configurations

It is well known that GGA-PBE functional does not account for the vdW interactions and tends to give overestimated values of binding energy. To accurately calculate the binding energies of different TATP configurations, we employ the DFT-D2 semiempirical correction[1] as implemented in the Siesta package.

Furthermore, as Siesta uses a set of localized atomic orbitals, it introduces the basis set superposition error (BSSE). The BSSE, if not taken into account, leads to the incorrect values of the binding energy. To alleviate this, we calculate binding energy using the counter-poise correction[2] using the following formula:

$$E_{binding}(SA) = \left(E(S_0) + E(A_0) - E(SA)\right) + \delta_{BSSE.}$$

The *E(SA)* is the total energy of the relaxed geometry of the given configuration (electrodes and molecule), while $E(S_0)$ and $E(A_0)$ are those of the individually relaxed geometries of electrodes and molecule, respectively. The δ_{BSSE} correction term is given by expression:

$$\delta_{BSSE} = (E_{SA}(A) - E_{SA}(SA_G)) + (E_{SA}(S) - E_{SA}(S_G A))$$.

The $E_{SA}(A)/E_{SA}(A)$ are the total energies of the electrodes/molecule with coordinates from the relaxed geometry of the configuration SA. The $E(SA_G)/E(S_G A)$ are total energies of the relaxed geometry of the configuration SA in which ghost orbitals are used to describe atomic species that belong to the molecule/electrodes, respectively.

Table S1 The binding energies of different TATP configurations, calculated using DFT-D2 with CP correction.

TATP configuration	$E_{binding}$ (eV)	TATP configuration	$E_{binding}$ (eV)
A_0	**0.024**	**D_0**	**0.041**
A_1	-0.302	D_1	0.087
A_2	0.014	**D_2**	**0.063**
A_3	**-0.008**	D_3	-0.015
A_4	-0.364	D_4	0.065
B_0	**0.064**	E_0	0.089
B_1	-0.305	E_1	0.087
B_2	**0.109**	E_2	0.129
B_3	**0.138**	E_3	0.081
B_4	-0.092	E_4	0.113
C_0	0.065		
C_1	0.031		
C_2	0.055		
C_3	0.047		

C_4 0.024

2. *I-V* characteristics of most probable TATP orientations

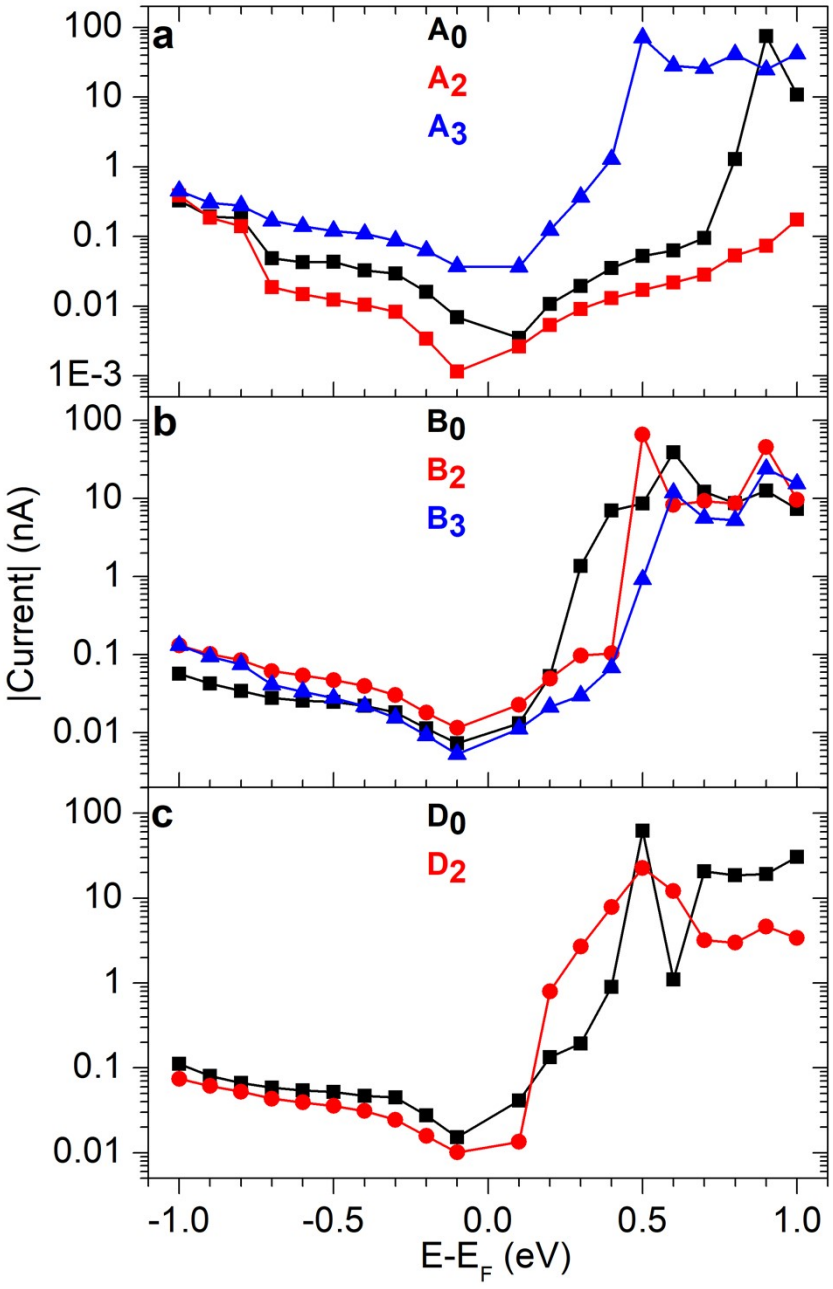

Figure S1 The *I-V* characteristics calculated using TranSiesta of configurations having weight w_i > 0.001: (a) A_0, A_2, and A_3 (black squares, red circles, blue triangles). (b) B_0, B_2, and B_3 (black squares, red circles, blue triangles). (c) D_0 and D_2 (black squares, red circles).

3. *I-V* characteristics of selected volatile organic compounds

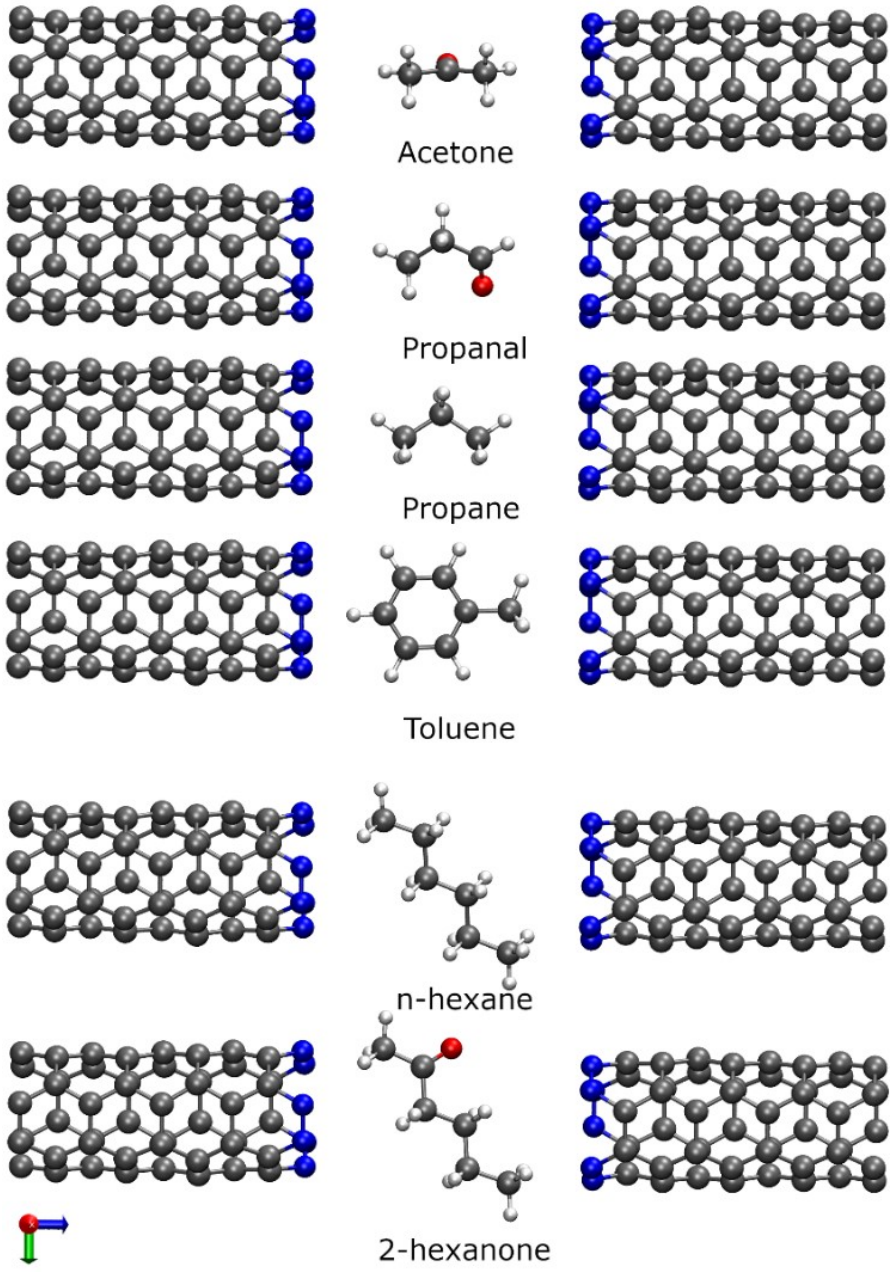

Figure S2 Relaxed geometries of prevalent volatile organic compounds placed in the gap between N-terminated (3,3) carbon nanotube electrodes.

We have limited our investigation of all VOCs but one, 2-hexanone, only to a single in-gap configuration. For acetone, propane, and propanal, we anticipate no change of in-gap position (orientation) to yield currents comparable to those of TATP due to their small size. In the cases of n-hexane and toluene, we calculated the transport characteristics of only one configuration because we do not expect the change of molecular position in the gap to induce significant molecule-electrode coupling necessary for the considerable electric current augmentation. Though large, these two molecules do not contain oxygen which enhances the molecule-electrode coupling, as will be shown in the next section.

4. Binding energies of VOCs

Table S2 The binding energies of VOCs, calculated using DFT-D2 with CP correction (see section 1).

VOC	$E_{binding}$ (eV)
toluene	0.248
2-hexanone	0.014
n-hexane	0.040
propane	0.102
propanal	0.107
acetone	0.102

5. The weighted average of *I-V* characteristics of 2-hexanone

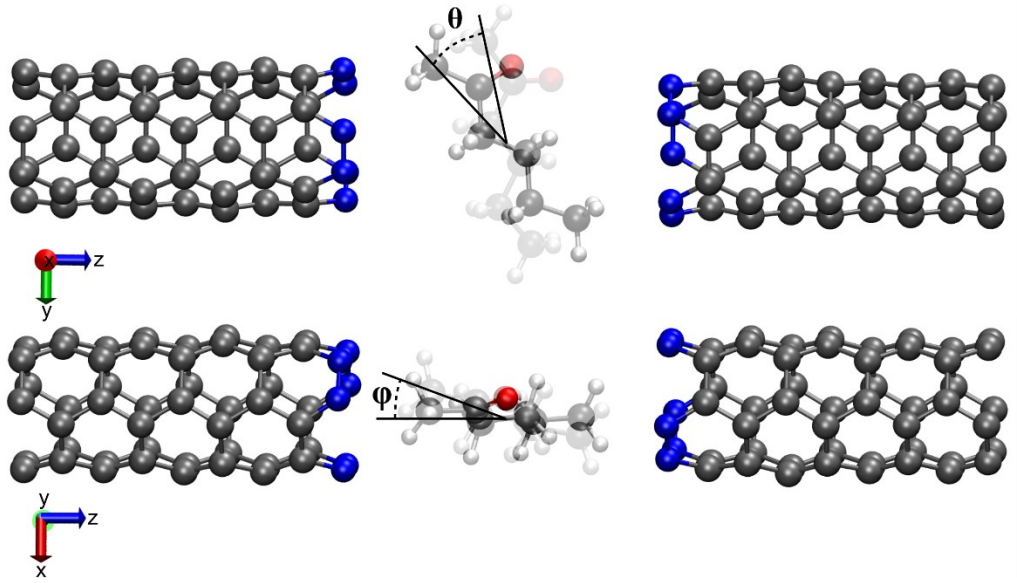

Figure S3 Angles ϑ and φ with respect to the geometry of 2-hexanone configuration X_0.

Following a similar procedure as in the case of the TATP, we examine different in-gap configurations of 2-hexanone. The new configurations are formed by rotations for angles ϑ and φ around the *x* and *y*-axis passing through the geometrical center of the molecule. The values of angles ϑ and φ are given with respect to the initial configuration X_0 (Fig. S3).

Table S3 The parameters of different in-gap configurations: angles before relaxation, the total energy of the system, and weight.

Configuration	ϑ_{in} [°]	φ_{in} [°]	E_i [eV]	w_i
X_0	0	0	-20483.52661	3.464E-05
X_1	0	-15	-20483.63065	1.924E-03
X_2	0	+15	-20483.57678	2.404E-04
X_3	30	0	-20483.40093	2.705E-07
X_4	30	-15	-20482.89728	9.703E-16
X_5	30	+15	-20482.89728	9.703E-16
X_6	**60**	**0**	**-20483.71435**	**4.871E-02**
X_7	**60**	**-15**	**-20483.7667**	**3.677E-01**
X_8	**60**	**15**	**-20483.76492**	**3.432E-01**
X_9	90	0	-20483.62324	1.445E-03
X_{10}	90	-15	-20483.58591	3.419E-04
X_{11}	**90**	**15**	**-20483.75526**	**2.364E-01**

The weighted average of the electric current of 2-hexanone (orange curve in Figure 3c) is at least an order of magnitude smaller than the one given in Figure 3b. The reason for such a discrepancy is that Figure 3b displays the curve for the highest-current position, not for the most probable one of the 2-hexanone in the nanogap.

6. The electronic transport of n-hexane and 2-henanone in N-terimnated CNT gaps

Both E_{HOMO} bias dependence and the spatial distribution of the HOMO wavefunction have a crucial influence on the transport properties. The evolution of E_{HOMO} of 2-hexanone with bias displays two distinct behaviors (bottom panel of Figure S4d): the strong pinning (SP)[3] at negative and the weak pinning (WP)[4] effect at positive bias. The SP characterizes the same variation with the voltage of the E_{HOMO} and the electrochemical potential of one of the electrodes: E_{HOMO} follows μ_L or μ_R. Conditions required to enter the SP regime are: (*i*) the spatial proximity (overlap) of the HOMO to one of the electrodes (CNTs), and (*ii*) the E_{HOMO} is almost the same as the electrochemical potential of that electrode[3]. The HOMO of 2-hexanone fulfills both conditions

and, thus, hybridizes with the left electrode at a negative bias (bottom panel of Figure S4d). The hybridization of HOMO with one of the electrodes leads to charge redistribution between the molecule and that electrode, and the molecule becomes (partially) charged with bias[3,5]. Indeed, at negative bias, the total Hirshfeld charge excess, Q_{MOL}, of all 2-hexanone atoms (top panel in Figure S4d) shows the charging effect. As voltage becomes more negative, the Q_{MOL} becomes more positive, keeping the E_{HOMO} out of the bias window (bottom panel of Figure S4d). Due to nonresonant transport in the SP regime, the electric current has low values (orange curve in Figure 3b).

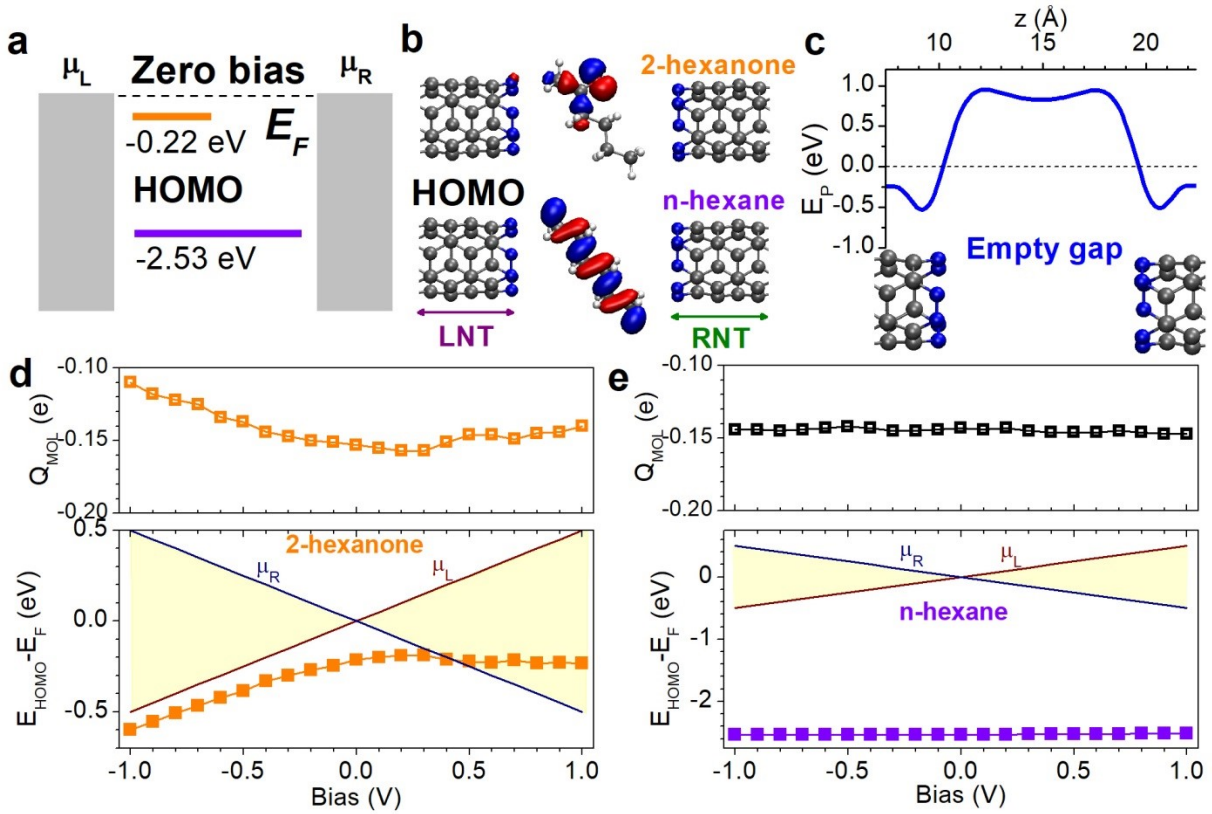

Figure S4 (a) The sketch of 2-hexanone (orange line) and n-hexane (purple line) HOMO energies with respect to the Fermi energy E_F (dashed line) of CNT electrodes at zero bias. (b) Spatial MPSH HOMO distribution of 2-hexanone (top panel) and n-hexane (bottom panel). The LNT and RNT are portions of the left and the right nanotube that belong to the central region. (c) The zero-bias electrostatic potential energy E_P along the midline in the z-direction in the gap between two (3,3) N-terminated CNTs. (d) Bias dependence of 2-hexanone HOMO energy $E_{HOMO} - E_F$ (bottom panel) and total Hirshfeld charge excess Q_{MOL} (top panel) on the molecule. (e) Bias dependence of n-hexane HOMO energy $E_{HOMO} - E_F$ (bottom panel) and total Hirshfeld charge excess Q_{MOL} (top panel) on the molecule. Wine and navy blue solid lines in the bottom panels of (d) and (e) denote bias dependence of the electrochemical potentials μ_L and μ_R of the left and the right electrode, respectively, and the light-yellow shaded regions represent the bias window.

At positive bias, E_{HOMO} barely changes with the voltage (bottom panel of Figure S4d), and since 2-hexanone HOMO is spatially closer to the left electrode, we observe no SP effect. In this case of weak pinning, there is no charge redistribution between the molecule and the electrode, and Q_{MOL} does not change with bias (top panel of Figure S4d). In the WP effect, the E_{HOMO} bias variation depends on the in-gap electrostatic potential and the spatial position of molecular HOMO[4]. The E_{HOMO} variation is more pronounced if HOMO is further from the center of the gap (top panel of Figure S4b) and is absent when HOMO has symmetrical spatial distribution around the gap center (bottom panel of Figure S4b)[4]. For 2-hexanone, E_{HOMO} slowly varies in the WP regime and enters the bias window at +0.5 V (bottom panel of Figure S4d), inducing a current jump (orange curve in Figure 3b) and the resonant transport.

In the case of n-hexane, while HOMO fulfills the condition of spatial proximity to both electrodes (bottom panel of Figure S4b), its energy is much smaller compared to μ_L and μ_R in the studied range of voltages (bottom panel of Figure S4e). Thus, we observe only a weak pinning regime in which E_{HOMO} (due to the uniform spread of the molecular HOMO around the center of the gap) and Q_{MOL} negligibly change with bias (Figure S4e). The nonresonant transport induces a low electric current and minor rectification (purple curve in Figure 3b).

7. Projected DOS of 2-hexanone

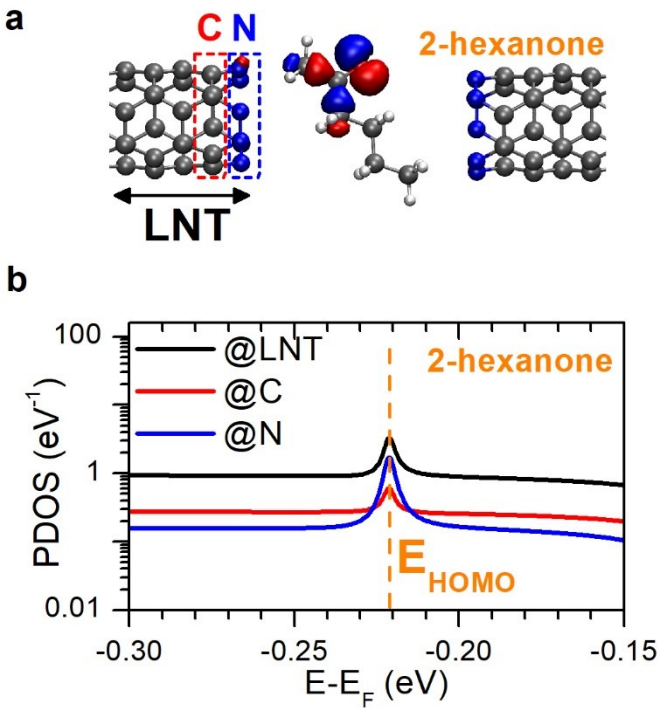

Figure S5 (a) Spatial MPSH HOMO distribution of 2-hexanone. The LNT marks the left nanotube atoms in the central region. Dashed rectangles denotes the layers of N (termination, blue) and

the adjacent C (red) atoms of the left CNT. (b) The PDOS at LNT (black) and layers of N (termination, blue) and the adjacent C (red).

8. Influence of the different CNT terminations on HOMO energy

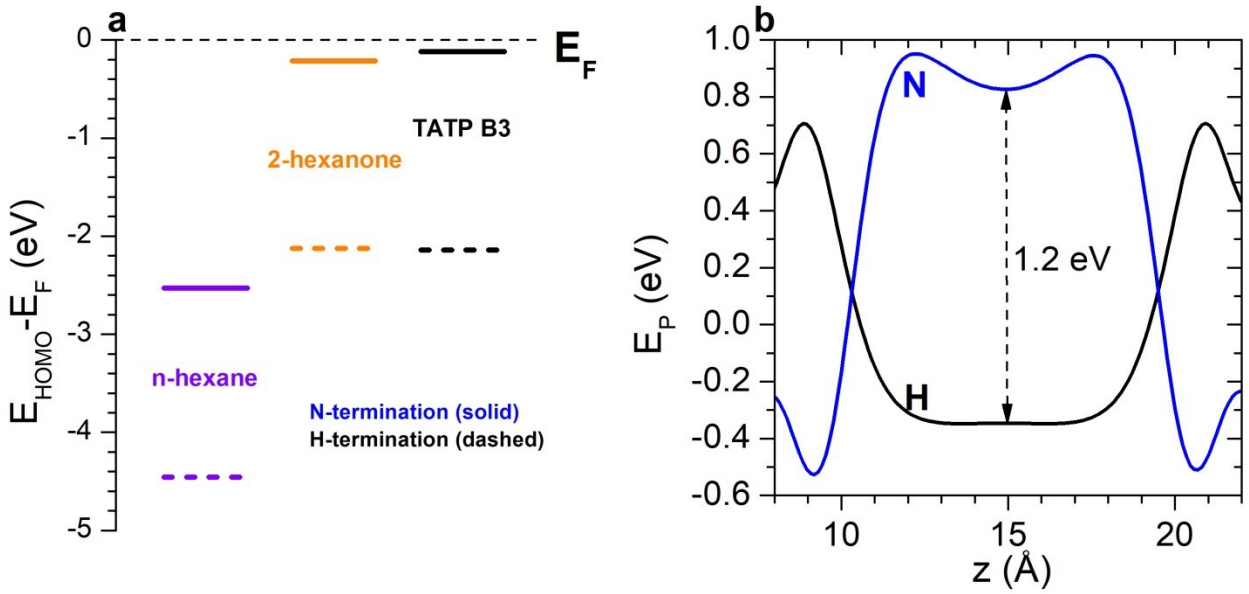

Figure S6 (a) E_{HOMO} with respect to E_F at zero bias of TATP B3 geometry (black), 2-hexanone (orange) and n-hexane (violet) in CNT gaps with N (solid) and H (dashed) termination. (b) The zero-bias electrostatic potential energy E_P along the midline in the *z*-direction in the gap between two (3,3) CNTs terminated with N (blue) and H (black).

9. Possibility for chemisorption of TATP at the end of N-terminated CNT

To check the possibility of TATP chemisorption at the end of N-terminated CNT electrodes we perform following calculations:

1) TATP molecule was moved toward the left electrode for 1 Å with respect to A_0 configuration, then the structure was relaxed. The relaxed configuration is practically the same as A_0, i. e. relaxation returns the molecule to the center of the gap.
2) TATP molecule was moved towards the left electrode for 1.5 Å with respect to A_0 configuration, then the structure was relaxed. The result is the same as in the first case.

3) TATP molecule was moved towards the left electrode for 1.5 Å with respect to A_0 configuration, then the relaxation was performed with fixed z coordinates of the TATP atoms. For this relaxed configuration, we have calculated the binding energy as described in the first section. The binding energy is E_b=-7.8 eV and it suggests unbinding.
4) TATP molecule was moved towards the left electrode for 2 Å with respect to A_0 configuration. The structure was relaxed and the result is shown in Figure S7a. The relaxed structure in Figure S7a has one N atom that has two bonds and one N atom that has four bonds, with H atom bound to it.
5) Finally, we modify the configuration in Figure S7a by attaching the H atom to the N atom that had just two bonds, so each of the N atoms has 3 bonds and we relax the new configuration (Figure S7b).

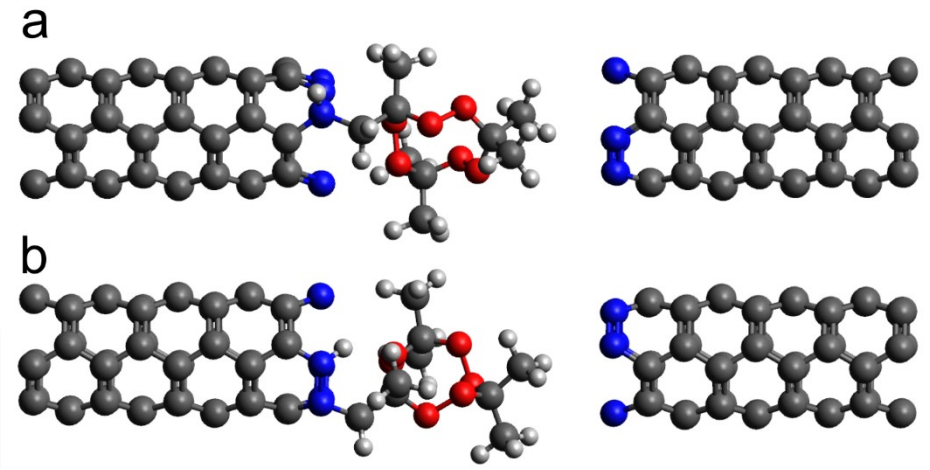

Figure S7 Two different configurations of the TATP molecule bound to the N-terminated electrode.

We then calculate the binding energy of these configurations: E_B(a) = 1.45 eV and E_B(b) = 2.77 eV. Although binding energies are large, it does not necessarily mean that those configurations will be realized. The question now is how likely is for those structures to form through a chemical reaction. We first assume that they are formed as products of chemical reactions of a single stationary nanotube and TATP molecules that pass through a nanopore, when incoming molecules collide with the nanotube. To estimate the rate constant (the number of successful collisions per second) of chemical reactions in which configurations from Figure S7 are formed we employ the Arrhenius equation

$$k = Ae^{-E_a/k_BT},$$

where A is the number of collisions per second (leading to a reaction or not), E_a is the activation energy for a chemical reaction, k_B is the Boltzmann constant and T is the temperature. To

estimate the activation energy, we refer to a recent paper on chemisorption of methane on N-terminated graphene[6], where two cases were observed:

1) methyl group and H atom bound to a single nitrogen (similar to our configuration in Figure S7a), and

2) the methyl group ends on one nitrogen and the H atom on the other (similar to our configuration in Figure S7b).

We assume that in our case activation energies are similar to the ones for graphene[6], i. e. E_a for the first is 1 eV and for the second is 1.5 eV, so the rate constants are

$$k(E_a = 1\ eV) = A * 4.4 * 10^{-18}$$ and

$$k(E_a = 1.5\ eV) = A * 9 * 10^{-27}.$$

Now we make an assumption that *A* would be equal to the number of TATP molecules that pass through a nanopore in 1 s so that every pass results in a collision. The exponent represents the probability that the collision will result in a reaction. If we assume that 10^6 TATP molecules would pass through a nanopore in 1s (A=10^6 s^{-1}), the value of the *k* would be equal to $4.4*10^{-12}$/ $9*10^{-21}$ successful collisions per second, making those a highly unlikely reactions at room temperature. This is in agreement with the study for adsorption of methane on N- terminated graphene where temperatures considered for reaction were over 900 K[6].

REFERENCES

1 S. Grimme, *J. Comput. Chem.*, 2006, **27**, 1787–1799.

2 S. F. Boys and F. Bernardi, *Mol. Phys.*, 1970, **19**, 553–566.

3 I. Djurišić, M. S. Dražić, A. Ž. Tomović, M. Spasenović, Ž. Šljivančanin, V. P. Jovanović and R. Zikic, *ACS Appl. Nano Mater.*, 2020, **3**, 3034–3043.

4 I. Djurišić, M. S. Dražić, A. Tomović, V. P. Jovanović and R. Zikic, *J. Nanoparticle Res.*, 2021, **23**, 1–8.

5 A. Z. Thong, M. S. P. Shaffer and A. P. Horsfield, *Nanoscale*, 2017, **9**, 8119–8125.

6 N. F. Xavier, G. F. Bauerfeldt and M. Sacchi, *ACS Appl. Mater. Interfaces*, 2023, **15**, 6951–6962.